analytical chemistry

pubs.acs.org/ac Article

DNA Structure Transition-Induced Affinity Switch for Biosensing Based on the Strong Electrochemiluminescence Platform from Organic Microcrystals

Ni Liao, Jia-Li Liu, Ya-Qin Chai, Ruo Yuan, and Ying Zhuo*

Cite This: *Anal. Chem.* 2020, 92, 3940−3948 Read Online

ACCESS | Metrics & More | Article Recommendations | Supporting Information

ABSTRACT: Here we described an effective recognition strategy using the target-triggered DNA structure transition as an affinity switch for nucleic acid detection based on the strong electrochemiluminescence (ECL) platform of 9,10-diphenylanthracene (DPA) doped perylene (Pe) microcrystals (DPA@Pe MCs). Specifically, the target-triggered rolling-circle amplification (RCA) could generate a long, single-stranded DNA with repeated G-quadruplex units, which would hinder the access of quenching probes due to the steric hindrance effects offered by the DNA structure transition. Using this effective recognition strategy, an ECL biosensor with ultrasensitive and accurate characteristics was proposed to detect microRNA-21, which showed an excellent linear response from 10 aM to 1 pM with the detection limit down to 4.14 aM. The DNA structure transition-induced affinity switch strategy offered a potential applications in clinical diagnosis analysis.

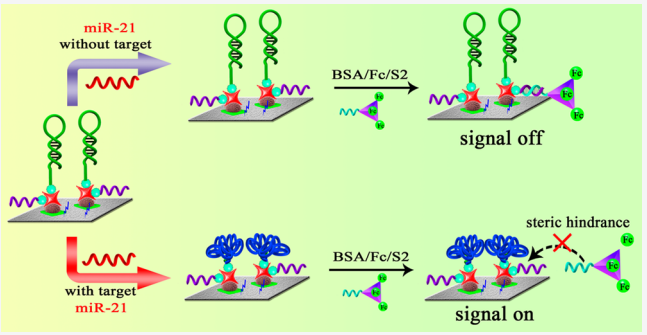

The development of a convenient, sensitive, and accurate recognition strategy is of great significance in proteomics and clinical diagnostics.[1−4] Typically, the direct molecule recognition was dependent on the label of the affinity ligands (such as antibodies, DNA, or aptamers) with photo/electric active materials for signal output. However, these methods may suffer from low selectivity, leading to the significant nonspecific signal. Recently, there was widespread interest in the development of an effective affinity switch for highly sensitive biological macromolecule detection. Usually, an affinity switch that exploits steric hindrance effects could remarkably improve the specificity and selectivity for other coexisting macromolecules. For example, Jiang's group[5] developed an affinity switch based on the specific interaction between the target protein and fluorophore labeled aptamer, which might dramatically increase steric hindrance to protect fluorescence (FL) from accessing and quenching by the quenching probes. Vallée-Bélisle's group described[6] the switch strategy to detect a macromolecule by a signaling DNA strand bound to the macromolecule resulting in the steric hindrance effects, which inhibited the DNA strand to hybridize with a complementary strand attached to the surface of the electrode. These methods commonly rely on the innate steric hindrance from the target biomacromolecules. However, the biomarkers (such as DNA, microRNAs) without enough steric hindrance were difficult to detect with the above strategy. Drawing inspiration from the tailorability and editability of the nucleic acid structure,[7−9] we developed a novel recognition strategy for the small molecule (DNA or microRNAs) using the DNA structure transition as an affinity switch, which took the advantages of the target-triggered steric hindrance effects of the nucleic acid amplification strategy for specificity and selectivity enhancement. To the best of our knowledge, there is no report on the DNA structure transition-induced affinity switch for biosensor constructions.

Electrochemiluminescence (ECL) with high sensitivity, controllability, and a signal-to-noise ratio has aroused great interest in low abundance analyte analysis.[10−12] Substantial efforts have been contributed to explore the novel ECL luminophores with high stability and excellent controllability, such as quantum dots,[13,14] metal nanoclusters[15,16] and microcrystals of organic materials.[17] Recently, the microcrystals of polycyclic aromatic hydrocarbons (PAHs) and its derivates were particularly attractive for ECL-based bioanalytical applications due to the excellent FL quantum efficiency, low cost, and stable radical ions. In particular, the microcrystals of PAHs with non-coplanar structures exhibited aggregation-induced electrochemiluminescence (AI-ECL) in aqueous media compared with that in a dispersed state because the aggregation state in microcrystals may tend to aggregate

Received: December 1, 2019
Accepted: February 10, 2020
Published: February 10, 2020

https://dx.doi.org/10.1021/acs.analchem.9b05433
Anal. Chem. 2020, 92, 3940−3948

Scheme 1. Schematic Illustration of the Preparation of the DPA@Pe MCs (A), the Fabrication Process of the Biosensor and the Detection Mechanism Based on the Affinity Switch (B), and the Principle to Generate Steric Hindrance Effects by the Nucleic Acid Amplification Strategy (CHA and RCA Reaction) (C)

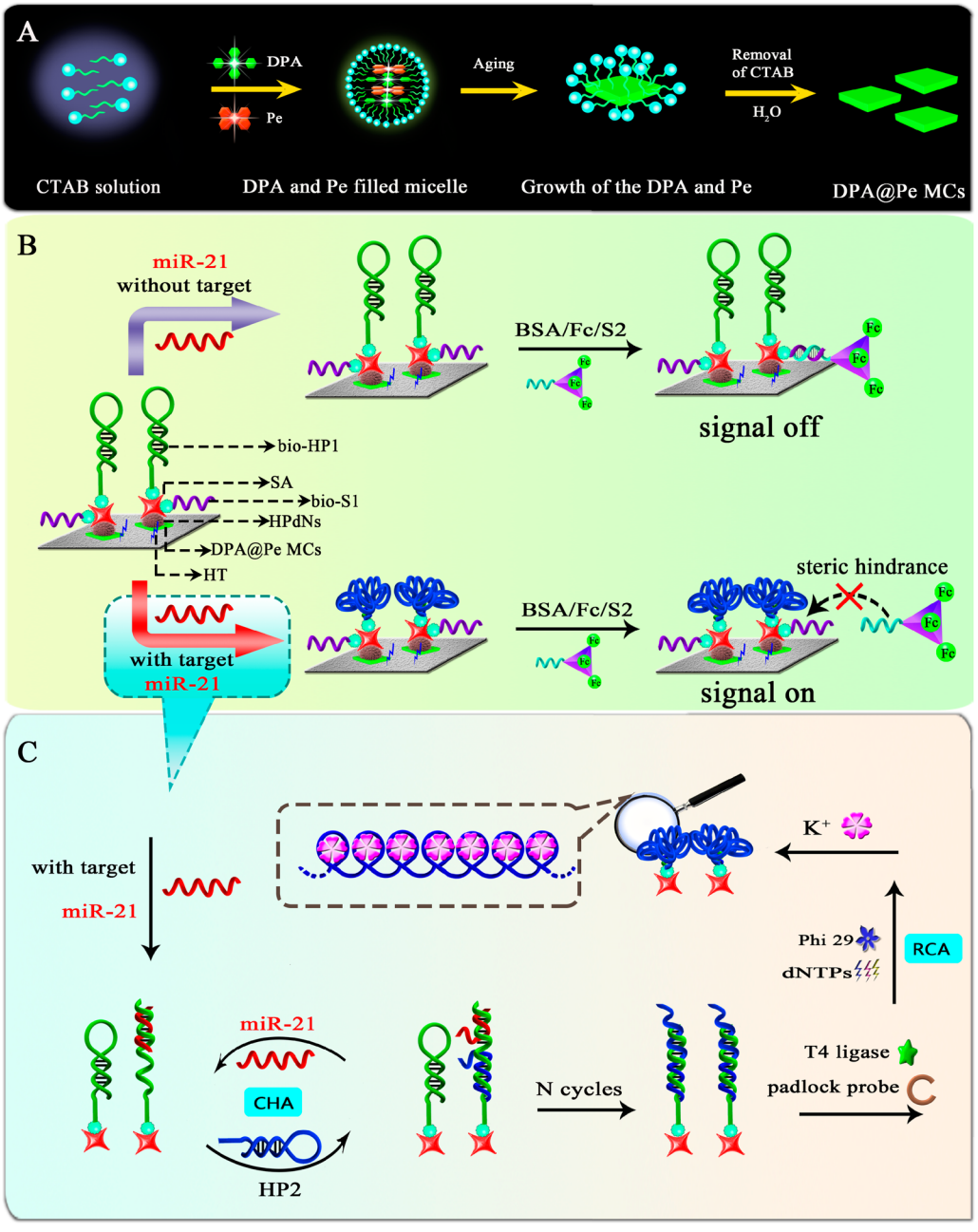

reduced energy gaps and limited intermolecular rotation. For example, a coumarin derivative, 6-[4-(*N*,*N*-diphenylamino)-phenyl]-3-ethoxycarbonyl coumarin, with weakly emissive or nonemissive ECL in a single molecule state has revealed strong emissions in the aggregate state,[18] which has been applied to the detection of small molecules. Recently, our group developed a sensitive ECL biosensor for mucin 1 detection using tetraphenylethylene nanocrystals (TPE NCs) as a novel AI-ECL emitter.[19] However, the ECL and FL emissions of coplanar PAHs molecules, such as perylene (Pe), were weakened or even quenched in the aggregation state due to the extremely strong $\pi-\pi$ interaction (named the aggregation-caused quenching effect, ACQ).[20,21] In this work, we developed a facile method to minimize the ACQ effect by preparing 9,10-diphenylanthracene (DPA) doped perylene (Pe) microcrystals (DPA@Pe MCs) to regulate the $\pi-\pi$ stacking, which exhibited a stronger ECL response than that of the pure Pe in the aggregated state and dispersed state. This strategy was the first example to avoid ACQ by changing the spatial arrangements of Pe molecules in microcrystals, which achieved a strong ECL of DPA@Pe MCs and may open more avenues for the further application of the planar PAHs with ACQ.

Herein, we first proposed the target-induced DNA structure transition as an affinity switch for the detection of microRNA 21 (miR-21) based on the DPA@Pe MCs as a new type of ECL emitter. The construction steps of the proposed biosensor were shown in Scheme 1. Briefly, the DPA@Pe MCs and

https://dx.doi.org/10.1021/acs.analchem.9b05433
Anal. Chem. 2020, 92, 3940−3948

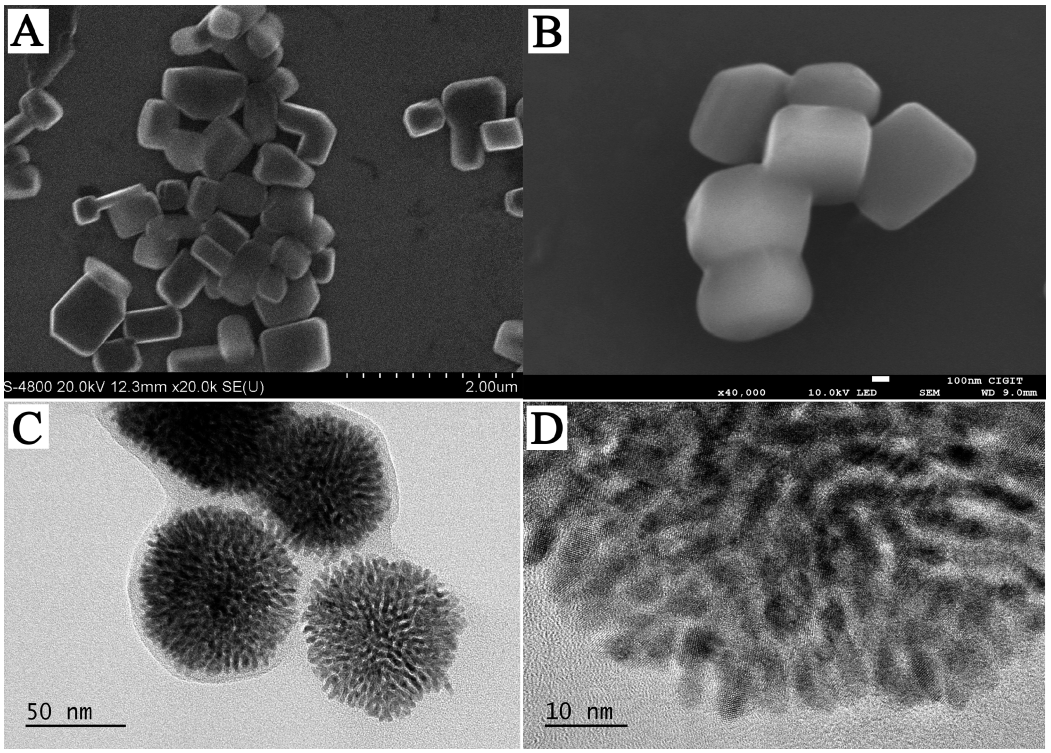

Figure 1. (A) SEM images of the DPA@Pe MCs. (B) The enlarged SEM image of DPA@Pe MCs. (C) TEM images of the HPdNs. (D) The enlarged TEM image of HPdNs.

hollow palladium nanospheres (HPdNs) were dropped on the electrode surface successively to immobilize streptavidin (SA) via a Pd−S bond, which could capture biotinylated single-strand S1 (bio-S1) and biotinylated hairpin probe 1 (bio-HP1). In the presence of miR-21, the bio-HP1 was opened and initiated the target circle with the help of hairpin probe 2 (HP2) (the process was described as a catalyzed hairpin assembly, abbreviated as CHA, part C in Scheme 1). Meanwhile, the products of CHA offered the single-stranded structure as rolling-circle amplification (RCA) primers. Subsequently, long DNA sequences with repeated G-quadruplex units were produced by RCA reaction, which acted as a signal competitor to hinder the access of ECL quenching probes (bovine albumin labeled with both ferrocene and the DNA strand S2, abbreviated as BSA/Fc/S2) due to the steric hindrance effects offered by the DNA structure transition. The developed biosensor could perform the ultrasensitive detection of miR-21 based on a DNA structure transition-induced affinity switch, which started a new chapter for the detection of a small-molecule target.

EXPERIMENTAL SECTION

Preparation of DPA@Pe MCs. The reprecipitation method was used to synthesize the DPA@Pe MCs with some modifications.[22] First, 2 mg of DPA powder and 2 mg of Pe powder were dissolved in 2 mL of tetrahydrofuran (THF) solution with vigorous stirring to prepare a homogeneous mixture solution (1 mg/mL) containing DPA and Pe. Following that, the mixture solution was rapidly injected into 5 mL of hexadecyl trimethylammonium bromide (CTAB) solution (15 mM) with a moderate stirring speed of 10000 rpm for 20 min. After centrifugation, the DPA@Pe MCs were collected and washed several times by deionized water. Ultimately, the DPA@Pe MCs were redispersed in 5 mL of deionized water for subsequent use.

Synthesis of Quenching Probes (BSA/Fc/S2). The quenching probes (abbreviated as BSA/Fc/S2) were prepared by covalently cross-linking BSA with ferrocenecarboxylic acid and S2 (5′-NH_2-modified DNA strand) by a facile one-pot method with the help of 1-ethyl-3-(3-(dimethylamino)propyl carbodiimide) hydrochloride (EDC) and *N*-hyroxysuccinimide (NHS). Briefly, 1 mL of 4 mg/mL ferrocenecarboxylic acid ethanol solution and 1 mL of 4 μM S2 were mixed with 2 mL of 5% BSA under stirring for 0.5 h. Then, 1 mL of the mixture solution of EDC and NHS (with an EDC: NHS ratio of 4:1) was added into the above solution at 4 °C under stirring overnight to obtain the quenching probes. The resultant mixture was collected by centrifugation, washed with deionized water several times, and then dispersed in 2 mL of deionized water and stored at 4 °C for further use.

Fabrication of the ECL Biosensor. First, the bare glassy carbon electrode (GCE, Φ = 4 mm) was pretreated as described in the published method.[23] To obtain the DPA@Pe MCs-modified electrode (DPA@Pe MCs/GCE), 10 μL of DPA@Pe MCs solution was dropped on the GCE surface and dried in air. Afterward, 10 μL of HPdNs solution was assembled on DPA@Pe MCs/GCE through electrostatic interaction. Subsequently, 10 μL of SA (0.1 mg/L) solution was dropped on the modified HPdNs/DPA@Pe MCs/GCE, described above, via a Pd−S bond (SA/HPdNs/DPA@Pe MCs/GCE). After being rinsed with deionized water, the resultant electrode was incubated in 10 μL of hexanethiol (HT, 1.0 mM) for 40 min at room temperature to eliminate the nonspecific binding effect. Then, 10 μL of the mixture solution contanining 2 μmol/L biotin-HP1 and 2 μmol/L biotin-S1 was dropped on the resultant electrode at 37 °C for 30 min via specific binding between biotin and SA. Ultimately, the

https://dx.doi.org/10.1021/acs.analchem.9b05433
Anal. Chem. 2020, 92, 3940−3948

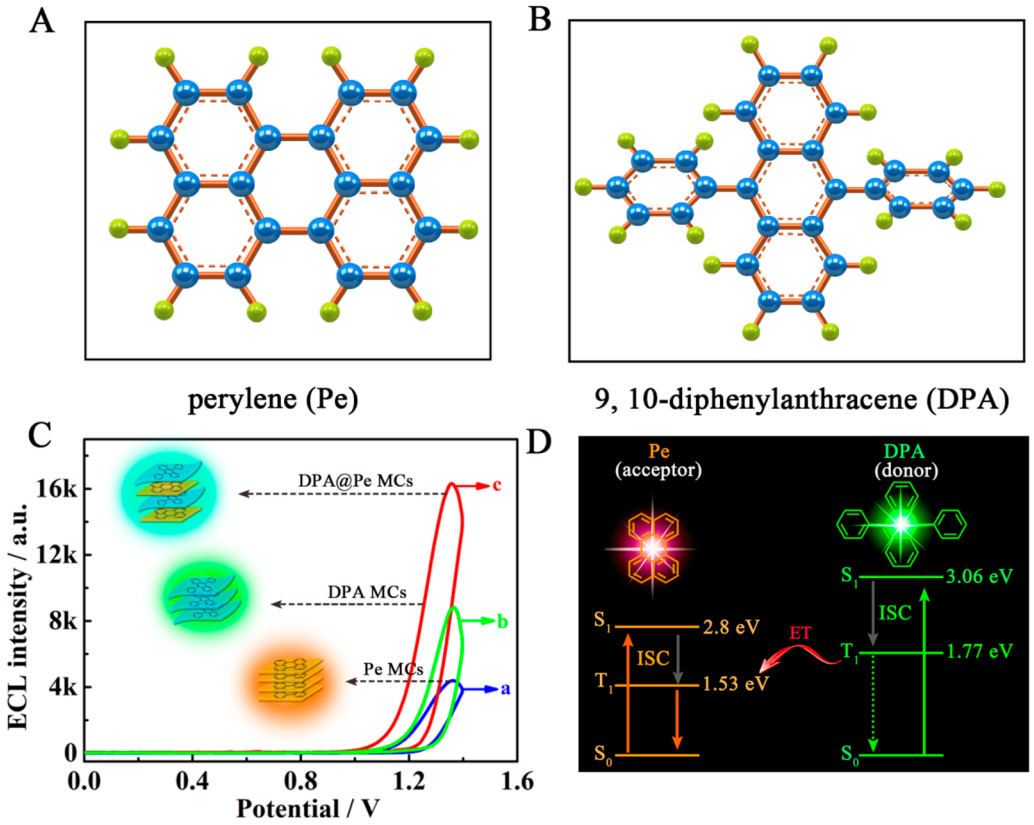

Figure 2. Structures of Pe molecule (A) and DPA molecule (B). The ECL−potential profiles of different microcrystal-modified GCE in 2 mL of PBS containing 18 mmol/L TEA (C). The inset of part C showed a schematic diagram of the possible spatial arrangements from the different microcrystals. Energetic diagram of DPA and Pe molecules (D). S_0, ground state; S_1, first excited singlet state; T_1, first excited triplet state; ISC, intersystem crossing; ET, energy transfer.

prepared biosensor (bio-HP1+bio-S1/HT/SA/HPdNs/DPA@Pe MCs/GCE) was stored in 4 °C for the subsequent use.

Measurement Procedure. The sample solution was obtained by mixing 10 μL of HP2 (4 μM) and 10 μL of miR-21 with different concentrations. Subsequently, the fabricated biosensor (bio-HP1+bio-S1/HT/SA/HPdNs/DPA@Pe MCs/GCE) was incubated with 10 μL of sample solution at 37 °C to execute the target-induced CHA process. After deionized water cleaning, 10 μL of the mixture solution containing the 100 nM rationally designed padlock probe, 100 U/mL phi29 DNA polymerase, and 2.5 mM dNTPs was dropped onto the modified electrode surface at 37 °C for 90 min to initiate the RCA reaction, which generated a long DNA chain. It could provide the controllable steric hindrance to act as a signal competitor for the protection of ECL from accessing and quenching by the quenching probes. Finally, the resultant electrode was incubated with 10 μL of quenching probes at 4 °C for 4 h to hybridize with the bio-S1. After rinsing with deionized water, the biosensor was measured in phosphate buffer saline (PBS) containing 18 mM triethylamine (TEA), where the working potential was from 0 to 1.4 V (vs Ag/AgCl) and the scan rate was 0.3 V/s.

RESULTS AND DISCUSSION

Morphological Characterization of Different Nanomaterials. The morphologies of as-synthesized DPA@Pe MCs and HPdNs were characterized by scanning electron microscopy (SEM) and transmission electron microscopy (TEM), respectively. As illustrated in Figure 1A, the SEM images of DPA@Pe MCs showed the typical block structure, which had formed a smooth surface morphology with ∼300 nm in length and ∼200 nm in width. The enlarged SEM image of DPA@Pe MCs was shown in Figure 1B. The TEM images revealed that HPdNs possessed a porous nanostructure chiseled with a diameter of approximately 50 ± 20 nm, as shown in Figure 1C,D.

ECL Performance of the DPA@Pe MCs. First, the molecule structures of Pe and DPA were displayed in Figure 2A,B, respectively. Compared with the two-dimensional planar structure of the Pe molecule (Figure 2A), the DPA molecule in Figure 2B showed a non-coplanar structure such that the two phenyl side groups were situated out of the plane of the anthracene core. It was reported that the Pe microcrystals (Pe MCs) assembled through strong π−π stacking might suffer from the ACQ effect due to their planar aromatic structure.[21] Thus, we hypothesized the DPA as a kind of non-coplanar molecule that could regulate the molecular stacking fashions and reduce the ACQ effect of Pe. Herein, the ECL characteristics of the different microcrystal-modified GCE (abbreviated as Pe MCs/GCE, DPA MCs/GCE, and DPA@Pe MCs/GCE, respectively) were investigated under the same experimental conditions, and the corresponding ECL−potential profiles were illustrated in Figure 2C. The ECL intensities of Pe MCs/GCE (curve a) and DPA MCs/GCE (curve b) were observed at 4347 and 8826 au, which demonstrated that both of them can act as ECL emitters. More interestingly, a remarkably enhanced ECL signal of DPA@Pe MCs/GCE was reached at about 16332 au, which

https://dx.doi.org/10.1021/acs.analchem.9b05433
Anal. Chem. 2020, 92, 3940−3948

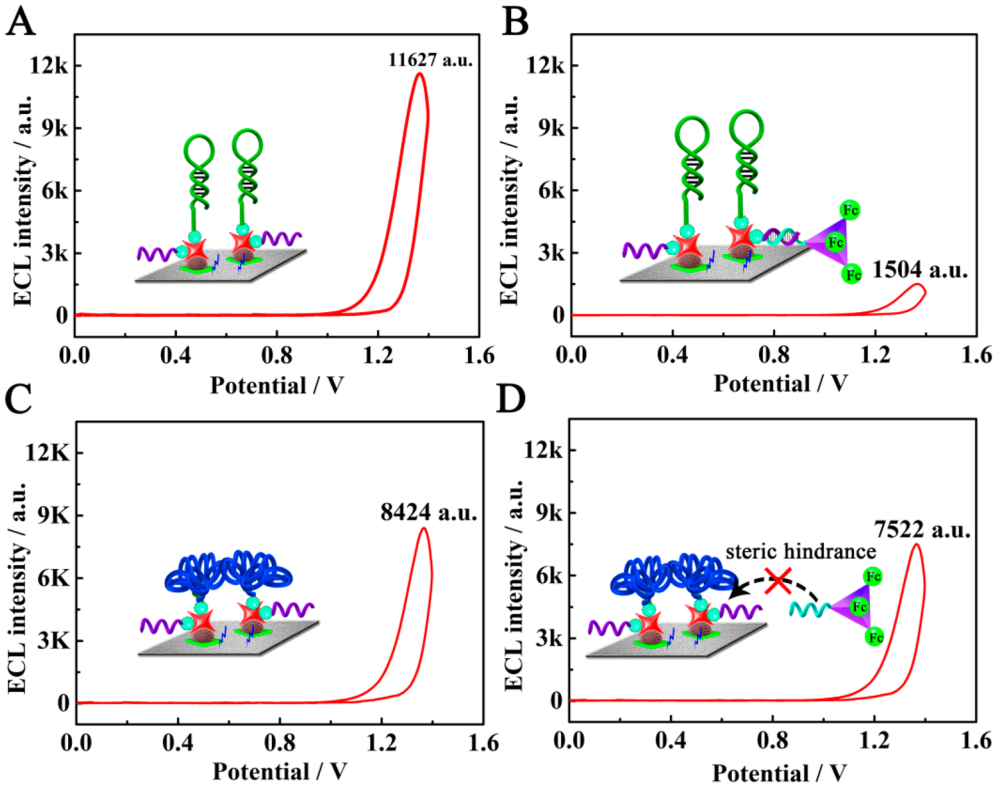

Figure 3. ECL responses of the proposed biosensor (bio-S1+bio-HP1/HT/SA/HPdNs/DPA@Pe MCs/GCE) (A), biosensor A executed the CHA and RCA reaction without target miR-21 and further incubated with quenching probes (B), biosensor A incubated with target miR-21 and executed the CHA and RCA reaction (C), and biosensor C incubated with quenching probes (D). Detection solution: 2 mL of PBS containing 18 mM TEA.

was 3.76-fold and 1.85-fold higher than that of Pe MCs/GCE and DPA MCs/GCE, respectively. In order to confirm which is the dominant ECL emitter in DPA@Pe MCs, the energetic diagrams of DPA and Pe were displayed in Figure 2D. It could be found that DPA with a higher E_{T1} (1.77 eV) and E_{S1} (3.06 eV)[24,25] could act as the donor, and Pe with lower E_{T1} (1.53 eV) and E_{S1} (2.80 eV)[26,27] could act as the acceptor in the DPA@Pe MCs. Consequently, there was energy transfer (ET) from DPA to Pe in the ECL process of DPA@Pe MCs. This demonstrated that the doping of DPA molecules could not only suppress the $\pi-\pi$ stacking of Pe molecules in microcrystal but also act as the donor to promote the ET from DPA to Pe resulting in an intense ECL emission. Furthermore, the DPA@Pe MCs/TEA system showed a higher relative ECL efficiency (~3.79 times) compared with that of the Pe MCs/TEA system (the detailed formula was shown in section S1.9 of the Supporting Information).

Feasibility Analysis of miR-21 Detection with Proposed Method. To demonstrate the feasibility of this recognition strategy, the ECL responses of the modified electrode incubated with the quenching probes with and without the signal competitor were recorded under the same experimental conditions. Before the incubation with sample solution, the ECL signal of the proposed biosensor (bio-S1+bio-HP1/HT/SA/HPdNs/DPA@Pe MCs/GCE) was about 11627 au (Figure 3A), indicating the strong ECL of DPA@Pe MCs. When the proposed biosensor was executed, as the CHA and RCA reaction without a target, a relatively low ECL intensity about 1504 au (Figure 3B) was obtained as the blank signal. It could be assigned to the lack of signal competitor, resulting in the ECL quenching probes accessing to the electrode surface. Compared with that of Figure 3A, the ECL intensity decreased in Figure 3C when the proposed biosensor was executed with the CHA and RCA reaction in the presence of the target miR-21, which was attributed to the steric hindrance caused by the RCA products. When the electrode of Figure 3C was further incubated with the quenching probes, an ECL intensity about 7522 au was obtained, as shown in Figure 3D. Compared with that of Figure 3B, the stronger ECL intensity was achieved with the target miR-21 under the same experimental process, because the RCA products prevented quenching probes from accessing the electrode surface. The feasibility of the developed biosensor was also confirmed by the polyacrylamide gel electrophoresis (PAGE) analysis; the results were shown in section S1.8 of the Supporting Information. These findings disclosed that the DNA structure transition-induced affinity switch might create a new methodology for developing biosensors for sensitive detection.

Comparison of the Sensitivities with Different Signal Switches. With the target concentration increasing, more RCA products were generated to produce large steric hindrance effects, which would act as a signal competitor to impede the ECL signal and prevent the quenching probes assessing the electrode surface. In order to compare the sensitivities with different signal switches between the signal competitor and the quenching probes, the ECL signals were recorded before and after the quenching probes were introduced. As shown in Figure 4A, the dotted line displayed the ECL responses of the proposed biosensor which executed the CHA and RCA reaction. Curves a, b, c in Figure 4A showed the ECL responses of the proposed biosensor toward

https://dx.doi.org/10.1021/acs.analchem.9b05433
Anal. Chem. 2020, 92, 3940−3948

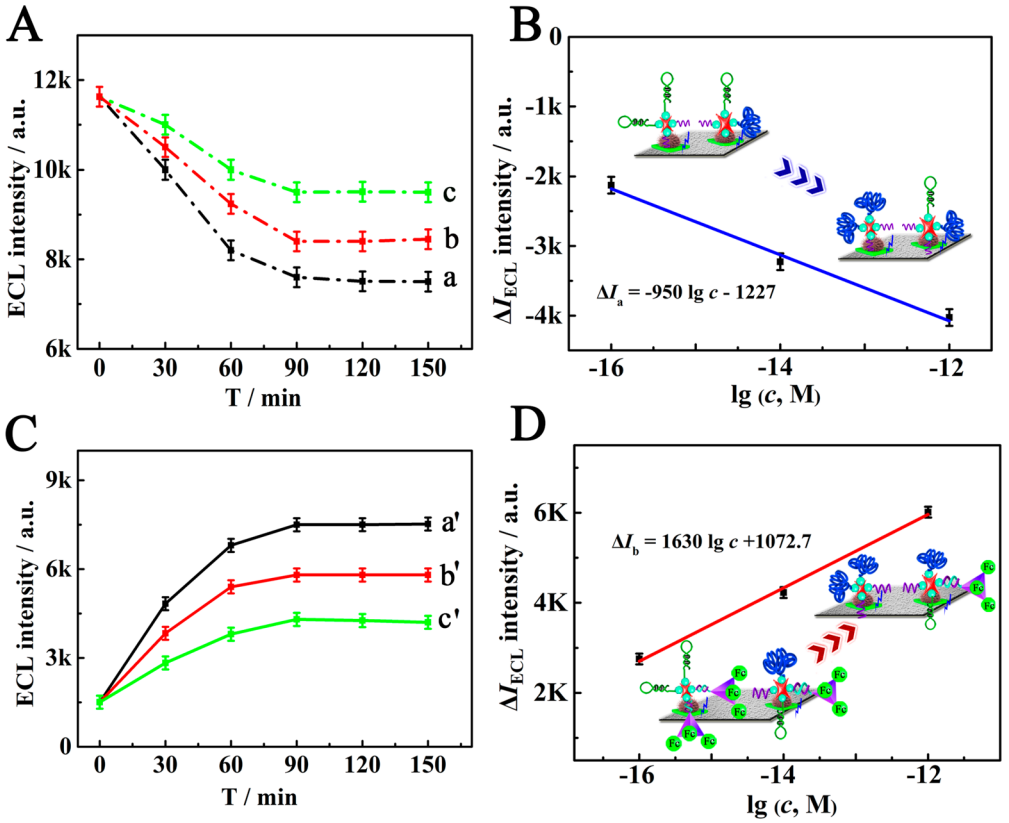

Figure 4. (A) ECL response vs RCA reaction time of the proposed biosensor (bio-S1+bio-HP1/HT/SA/HPdNs/DPA@Pe MCs/GCE) executed the CHA and RCA reaction (A), and further incubated with quenching probes (C). MiR-21 concentrations: (a, a′) 1 pM, (b, b′) 1.0×10^{-2} pM, (c, c′) 1.0×10^{-4} pM. The ECL changing trend with (D) and without (B) the quenching probes toward different concentrations of miR-21. Error bars, SD, $n = 3$.

the different concentrations of the target (1, 1.0×10^{-2}, 1.0×10^{-4} pM), respectively. With the increase in RCA reaction time, the ECL response kept a downward trend and stabilized eventually when the time was over 90 min. Moreover, the ECL signal of curve a decreased more significantly compared with that of curve c, because the RCA products led to the larger steric hindrance with increases in the concentration and the incubation time, which made the ECL signal decrease. The solid line in Figure 4C showed the ECL responses after the formation of the signal competitor and the incubation of the quenching probes. With the decrease in the target concentrations (1, 1.0×10^{-2}, 1.0×10^{-4} pM), the corresponding ECL response declined (curve a′, b′, c′ in Figure 4C), which could be assigned to fewer RCA products generated with the low target concentrations resulting in more quenching probes accessing the electrode surface. The results obviously illustrated that the larger steric hindrance produced by the long RCA reaction time resulted in fewer combined quenching probes, while the smaller steric hindrance produced by the shorter RCA reaction time resulted in more combined quenching probes. To summarize, the ECL response tended to be stable with the time up to 90 min; 90 min was chosen as the optimal incubation time of the RCA process. As displayed in Figure 4B,D, the lines represented the changing trend of ECL and different target concentrations before (Figure 4B) and after (Figure 4D) the incubation of quenching probes. Compared with the slope ($|k_a| = 950$) in Figure 4B, the slope in Figure 4D ($|k_b| = 1630$) exhibited a larger absolute value. It could be demonstrated that the biosensor was more sensitive when the ECL quenching probes were introduced.

Analytical Performance of the Biosensor. In order to achieve the optimal assay performance, the effect of CHA incubation time and the RCA incubation time on the proposed biosensor was investigated, and the results are shown in Figure S1. The linear response of the proposed biosensor was evaluated under the optimal conditions. As shown in Figure 5A, upon increasing the concentration of miR-21 (from 1.0×10^{-5} pM to 1.0 pM), the ECL response of the biosensor increased. Moreover, Figure 5B displayed the calibration plot with a good linear relationship between the ECL response and the logarithmic value of miR-21 concentrations. The regression equation was $\Delta I_{ECL} = 777.153 \lg c_{miR\text{-}21} + 13732$ with a correlation coefficient of 0.9971; the limit of detection was estimated to be 4.14 aM.

The selectivity was also investigated to assess the practicability and specificity of the developed biosensor for miR-21 detection. The developed biosensor was tested with different interference agents, including miR-155, miR-199A, and miR-141. As depicted in Figure 5C, in the presence of miR-21 (0.1 pM), the proposed biosensor displayed the strong ECL response compared with that of the blank solution (absence of target miR-21). However, a low ECL signal was obtained when miR-21 was replaced with miR-141 (10 pM), miR-155 (10 pM), and miR-199A (10 pM), respectively. After mixing the miR-155 (10 pM), miR-141 (10 pM), and miR-199A (10 pM) with the target miR-21(0.1 pM), the ECL responses showed no remarkable difference as compared to the effect of 0.1 pM miR-21 only. The results obviously illustrated that the proposed ECL biosensor has an excellent selectivity for miR-21 detection. Furthermore, the stability of the

https://dx.doi.org/10.1021/acs.analchem.9b05433
Anal. Chem. 2020, 92, 3940−3948

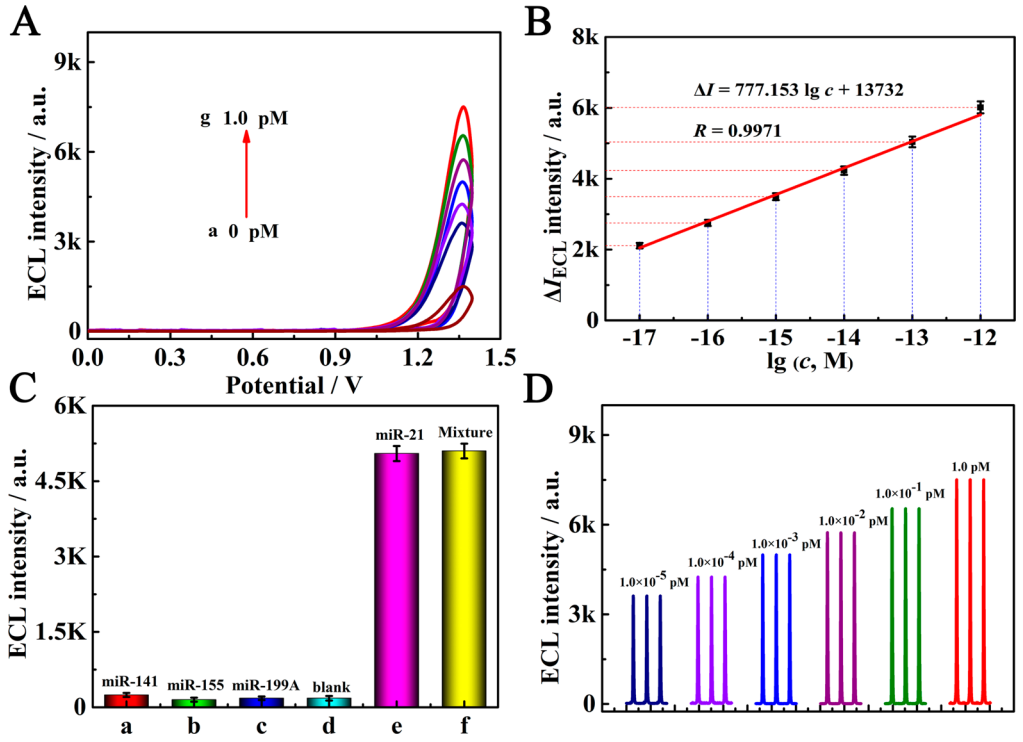

Figure 5. (A) ECL intensity−potential profiles of the designed biosensor with different concentrations of miR-21. Curves a−g: 0, 1.0×10^{-5}, 1.0×10^{-4}, 1.0×10^{-3}, 1.0×10^{-2}, 1.0×10^{-1}, and 1.0 pM. (B) Calibration plot of the ΔI_{ECL} intensity and the logarithm of miR-21 concentrations. (C) The selectivity of this method with different targets. (D) The ECL stability of the proposed biosensor with various concentrations of miR-21. Error bars, SD, $n = 3$.

proposed ECL biosensor was investigated, and the results are shown in Figure 5D. The ECL signal increased with the increase of miR-21 concentration correspondingly, and the stable ECL/time curves were obtained in different concentration ranges (from 1.0×10^{-5} pM to 1.0 pM) with the scan range 0−1.4 V and scan rate 0.3 V/s, which presented the favorable stability of the proposed biosensor.

Additionally, compared with that of the other test platforms (Table 1), the analytical performance of the prepared biosensor showed a high sensitivity for miR-21 detection.

Table 1. Comparison of Existing miRNA Detection Methods

method	detection	detection limit	ref
ECL	miRNA	0.03 fM	28
ECL	miRNA	10 fM	29
luminescence imaging	miRNA	12 fM	30
fluorescence	miRNA	47 pM	31
electrochemical	miRNA	1.6 fM	32
ECL	miRNA	4.14 aM	this work

Application of the Biosensor in Tumor Cells. To investigate the sensitive recognition of the developed biosensor for early cancer diagnosis, the tumor cell extractions of MCF-7 (the human breast adenocarcinoma cell line) were detected by the ECL biosensors to measure the expression of miR-21. As shown in Figure 6, curve b (blue x-axis), the developed biosensors exhibited good sensitivities by setting the cell concentrations from 10^1 cells to 10^6 cells, where the corresponding linear regression equation was $\Delta I_b = 772.26 \lg c_b + 1999.53$ ($k_b = 772.26$, c_b was the cell concentrations of

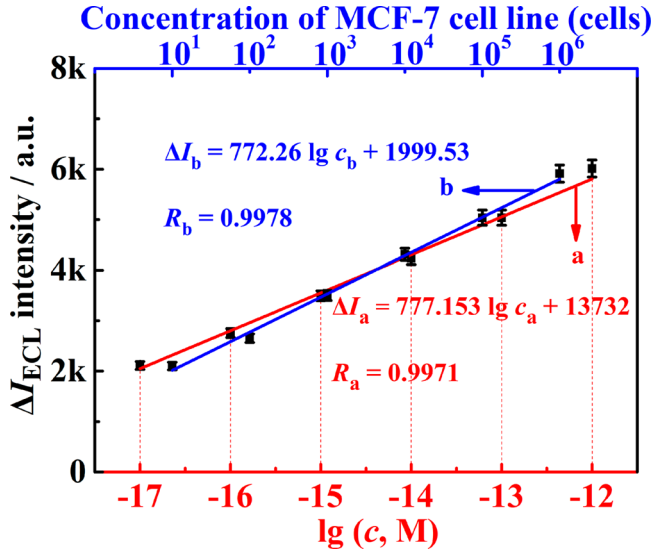

Figure 6. Application of the biosensor to detect miR-21 in MCF-7 and data analysis: 10^1 cells, 10^2 cells, 10^3 cells, 10^4 cells, 10^5 cells, and 10^6 cells.

MCF-7) with a correlation coefficient of $R_b = 0.9978$. As shown in Figure 6 (red x-axis), standard curve a was obtained when the prepared ECL biosensors were detected with the miR-21 standard solution, where the linear regression equation was $\Delta I_a = 777.153 \lg c_a + 13732$ ($k_a = 777.153$, c_a was the value of miR-21 concentration) with a correlation coefficient of $R_a = 0.9971$. As a result, calibration curve b exhibited an approximate slope with curve a ($k_a \approx k_b$).

https://dx.doi.org/10.1021/acs.analchem.9b05433
Anal. Chem. 2020, 92, 3940−3948

CONCLUSION

An ECL biosensor platform for sensitive monitoring of miR-21 was developed combining the merits of the affinity switch and DPA@Pe MC emitters. Concretely, target-triggered CHA and RCA reactions were employed to generate long DNA sequences for switch strategy construction, because the DNA structure transition could act as a signal competitor to hinder the access of quenching probes due to steric hindrance for specificity and selectivity improvement. At the same time, the significantly enhanced ECL from the DPA@Pe MCs-modified electrode was achieved in aqueous solutions due to the minimization of ACQ by changing the spatial arrangements of Pe molecules in microcrystals via the DPA doping. In summary, the proposed biosensor offered a sensitive, specific, and efficient platform for the microRNA detection quantitatively and opened up new horizons to design other organic microcrystals as emitters in ECL assays.

ASSOCIATED CONTENT

Supporting Information

The Supporting Information is available free of charge at https://pubs.acs.org/doi/10.1021/acs.analchem.9b05433.

Detailed methodological description of the reagents and materials, apparatus, pretreatment of DNA strands, hollow palladium nanospheres (HPdNs), applications for practical aample detection, optimization of the reaction conditions, ECL and EIS characterizations of the proposed biosensor, native polyacrylamide gel electrophoresis (PAGE), and the relative ECL efficiency of DPA@Pe MCs (PDF)

AUTHOR INFORMATION

Corresponding Author

Ying Zhuo − *Chongqing Engineering Laboratory of Nanomaterials & Sensor Technologies, College of Chemistry and Chemical Engineering, Southwest University, Chongqing 400715, China;* orcid.org/0000-0002-4491-1186; Phone: +86 23 68253172; Email: yingzhuo@swu.edu.cn; Fax: +86 23 68253172

Authors

Ni Liao − *Chongqing Engineering Laboratory of Nanomaterials & Sensor Technologies, College of Chemistry and Chemical Engineering, Southwest University, Chongqing 400715, China; College of Biological and Chemical Engineering, Panzhihua University, Panzhihua 617000, China*

Jia-Li Liu − *Chongqing Engineering Laboratory of Nanomaterials & Sensor Technologies, College of Chemistry and Chemical Engineering, Southwest University, Chongqing 400715, China*

Ya-Qin Chai − *Chongqing Engineering Laboratory of Nanomaterials & Sensor Technologies, College of Chemistry and Chemical Engineering, Southwest University, Chongqing 400715, China;* orcid.org/0000-0003-4392-9592

Ruo Yuan − *Chongqing Engineering Laboratory of Nanomaterials & Sensor Technologies, College of Chemistry and Chemical Engineering, Southwest University, Chongqing 400715, China;* orcid.org/0000-0003-3664-6236

Complete contact information is available at: https://pubs.acs.org/10.1021/acs.analchem.9b05433

Notes

The authors declare no competing financial interest.

ACKNOWLEDGMENTS

This work was financially supported by the NNSF of China (21675130, and 21775124), the Natural Science Foundation Project of CQ CSTC (cstc2018jcyjAX0546), and the Fundamental Research Funds for the Central Universities (XDJK2019TJ002), China

REFERENCES

(1) Kawatani, M.; Osada, H. *MedChemComm* **2014**, *5*, 277−287.
(2) Leslie, B. J.; Hergenrother, P. J. *Chem. Soc. Rev.* **2008**, *37*, 1347−1360.
(3) Pan, S. j.; Zhang, H. L.; Wang, C. Y.; Yao, S. C. L.; Yao, S. Q. *Nat. Prod. Rep.* **2016**, *33*, 612−620.
(4) Wright, M. H.; Sieber, S. A. *Nat. Prod. Rep.* **2016**, *33*, 681−708.
(5) Wang, H. Q.; Wu, Z.; Tang, L. J. *Nucleic Acids Res.* **2011**, *39*, e122.
(6) Mahshid, S. S.; Camiré, S.; Ricci, F.; Vallée-Bélisle, A. *J. Am. Chem. Soc.* **2015**, *137*, 15596−15599.
(7) Lu, L. M.; Zhang, X. B.; Kong, R. M.; Yang, B.; Tan, W. H. *J. Am. Chem. Soc.* **2011**, *133*, 11686−11691.
(8) Li, Y.; Teng, X. C.; Zhang, K. X.; Deng, R. J.; Li, J. H. *Anal. Chem.* **2019**, *91*, 3989−3996.
(9) Ge, L.; Wang, W. X.; Sun, X. M.; Hou, T.; Li, F. *Anal. Chem.* **2016**, *88*, 9691−9698.
(10) Liu, Z.; Qi, W.; Xu, G. *Chem. Soc. Rev.* **2015**, *44*, 3117−3142.
(11) Voci, S.; Goudeau, B.; Valenti, G.; Lesch, A.; Jović, M.; Rapino, S.; Paolucci, F.; Arbault, S.; Sojic, N. *J. Am. Chem. Soc.* **2018**, *140*, 14753−14760.
(12) Tan, X.; Zhang, B.; Zou, G. Z. *J. Am. Chem. Soc.* **2017**, *139*, 8772−8776.
(13) Feng, L. L.; Wu, Y. X.; Zhang, D. L.; Hu, X. X.; Zhang, J.; Wang, P.; Song, Z. L.; Zhang, X. B.; Tan, W. H. *Anal. Chem.* **2017**, *89*, 4077−4084.
(14) Li, H. Y.; Wang, C. F.; Hou, T.; Li, F. *Anal. Chem.* **2017**, *89*, 9100−9107.
(15) Yang, F.; Zhong, X.; Jiang, X. Y.; Zhuo, Y.; Yuan, R.; Wei, S. P. *Biosens. Bioelectron.* **2019**, *130*, 262−268.
(16) Peng, H. P.; Huang, Z. N.; Sheng, Y. L.; Zhang, X. P.; Deng, H. H.; Chen, W.; Liu, J. W. *Angew. Chem., Int. Ed.* **2019**, *58*, 11691−11694.
(17) Han, Z. G.; Yang, Z. F.; Sun, H. S.; Xu, Y. L.; Ma, X. F.; Shan, D. L.; Chen, J.; Huo, S. H.; Zhang, Z.; Du, P. Y.; Lu, X. Q. *Angew. Chem., Int. Ed.* **2019**, *58*, 5915−5919.
(18) Liu, H. W.; Wang, L. F.; Gao, H. F.; Qi, H. L.; Gao, Q.; Zhang, C. X. *ACS Appl. Mater. Interfaces* **2017**, *9*, 44324−44331.
(19) Jiang, M. H.; Li, S. K.; Zhong, X.; Liang, W. B.; Chai, Y. Q.; Zhuo, Y.; Yuan, R. *Anal. Chem.* **2019**, *91*, 3710−3716.
(20) Zhao, Z.; Gao, S. M.; Zheng, X. Y.; Zhang, P. F.; Wu, W. T.; Kwok, R. T. K.; Xiong, Yu.; Leung, N. L. C.; Chen, Y. C.; Gao, X. K.; Lam, J. W. Y.; Tang, B. Z. *Adv. Funct. Mater.* **2018**, *28*, 1705609.
(21) Huang, Y. j.; Xing, J.; Gong, Q. Y.; Chen, L. C.; Liu, G. F.; Yao, C. J.; Wang, Z. R.; Zhang, H. L.; Chen, Z.; Zhang, Q. C. *Nat. Commun.* **2019**, *10*, 169.
(22) Liu, J. L.; Tang, Z. L.; Zhang, J. Q.; Chai, Y. Q.; Zhuo, Y.; Yuan, R. *Anal. Chem.* **2018**, *90*, 5298−5305.
(23) Wu, F. F.; Zhou, Y.; Zhang, H.; Yuan, R.; Chai, Y. Q. *Anal. Chem.* **2018**, *90*, 2263−2270.
(24) Bharmoria, P.; Hisamitsu, S.; Nagatomi, H.; Ogawa, T.; Morikawa, M. A.; Yanai, N.; Kimizuka, N. *J. Am. Chem. Soc.* **2018**, *140*, 10848−10855.
(25) Chen, W. L.; Song, F. L.; Tang, S. L.; Hong, G. B.; Wu, Y. N.; Peng, X. J. *Chem. Commun.* **2019**, *55*, 4375−4378.
(26) Wang, Z.; Zhao, J.; Barbon, A.; Toffoletti, A.; Liu, Y.; An, Y.; Xu, L.; Karatay, A.; Yaglioglu, H. G.; Yildiz, E. A.; Hayvali, M. *J. Am. Chem. Soc.* **2017**, *139*, 7831−7842.

(27) Zhang, C.; Zhao, J.; Wu, S.; Wang, Z.; Wu, W.; Ma, J.; Guo, S.; Huang, L. *J. Am. Chem. Soc.* **2013**, *135*, 10566−10578.
(28) Zhang, P.; Li, Z. Y.; Wang, H. J.; Zhuo, Y.; Yuan, R.; Chai, Y. Q. *Nanoscale* **2017**, *9*, 2310−2316.
(29) Liao, Y. H.; Huang, R.; Ma, Z. K.; Wu, Y. X.; Zhou, X. M.; Xing, D. *Anal. Chem.* **2014**, *86*, 4596−4604.
(30) Li, C. Y.; Cao, D.; Song, C. Y.; Xu, C. M.; Ma, X. Y.; Zhang, Z. L.; Pang, D. W.; Tang, H. W. *Chem. Commun.* **2017**, *53*, 4092−4095.
(31) Zhen, S. J.; Xiao, X.; Li, C. H.; Huang, C. Z. *Anal. Chem.* **2017**, *89*, 8766−8771.
(32) Miao, X. M.; Wang, W. H.; Kang, T. S.; Liu, J. B.; Shiu, K.; Leung, C.; Ma, D. *Biosens. Bioelectron.* **2016**, *86*, 454−458.

https://dx.doi.org/10.1021/acs.analchem.9b05433
Anal. Chem. 2020, 92, 3940−3948